Renewable Energy 43 (2012) 292–300

Contents lists available at SciVerse ScienceDirect

Renewable Energy

journal homepage: www.elsevier.com/locate/renene

Influence of duct geometry on the performance of Darrieus hydroturbine

A.R. Malipeddi, D. Chatterjee*

Hydroturbomachines Laboratory, Department of Mechanical Engineering, Indian Institute of Technology Madras, Chennai 600036, India

ARTICLE INFO

Article history:
Received 24 June 2011
Accepted 24 December 2011
Available online 12 January 2012

Keywords:
Darrieus
Hydroturbine
Augmentation
Duct parameters

ABSTRACT

Computational study is carried out to develop a new duct with the purpose of improving the performance of a straight-bladed Darrieus hydroturbine. Though Darrieus turbine is very simple to construct, it has some disadvantages when compared to axial turbines. These are a lower power coefficient and a variation in the torque produced within the cycle leading to periodic loading on the components of the turbine. The main objective of the present study is to retain the simple design and fabrication procedure of Darrieus turbine while reducing the disadvantages. In this study, a new duct is developed, for a given turbine design, that reduces the variation in torque over a cycle by appropriately directing the flow upstream and downstream the turbine while increasing power conversion. At the operating point, which is at a tip-speed ratio of 2, use of a duct reduces the torque ripple by a factor of 4.15 and the power coefficient(C_p)is increased to 0.63 from 0.40. By choosing the position of the turbine in the duct appropriately, it is shown that the torque ripple may be reduced by a factor of 6.37, at the expense of the power coefficient. And, a maximum $C_p = 0.644$ is observed when the turbine center coincided with the throat of the duct. Similarly, the effect of varying other parameters such as the convergence angle of the duct and its external shape on the performance of the turbine are studied through numerical simulation. It is seen that there exists an optimum value in each case. While varying the convergence angle of the duct it is observed that the maximum power coefficient and lowest torque ripple are obtained at the same value of duct half angle, equal to 27°. The dependence of the power coefficient and torque ripple on duct convergence angle is weak. The duct with straight external shape is observed to have best performance with a peak power coefficient of 0.72, while the convex external shape has a peak of only 0.51. The external shape is observed to have a negligible effect of the torque ripple factor. Significance of the emerging trends of parameters are discussed.

1. Introduction

1.1. Hydrokinetic power

Hydrokinetic turbines convert the kinetic energy of the flow as opposed to conventional hydroturbines which operate under a potential energy difference created by use of dams. The sources for hydrokinetic energy are (a) rivers, streams, (b) tidal currents and (c) marine currents.

Darrieus turbine falls under the category of cross-flow turbines. Over the past couple of decades, hydrokinetic energy conversion has gained momentum and the use of Darrieus turbine for converting hydrokinetic energy is increasing [1]. It is used as an isolated unit for small applications and scaling up has been proposed by using an array of such vertical-axis turbines. The main drawbacks of Darrieus turbine are lower power coefficient compared to axial turbines and variation of the torque output (often termed as torque ripple).

Alternatives to the Darrieus turbine include the Gorlov turbine developed by Gorlov [2]. It uses helical blades in place of the straight blades used by Darrieus turbine. Gorban et al. [3] have studied the design proposed by Gorlov. Another turbine that has a reduced torque variation over the cycle is the Achard turbine studied by Bernad et al. [4]. It consists of a runner that has chevron-shaped blades oriented vertically.

However, one of the main advantages of the straight-bladed Darrieus turbine is its simplicity of construction, because of which it is very inexpensive. While the alternative options solve some of the problems associated with the Darrieus turbine, this comes at the cost of a complicated design which requires advanced manufacturing techniques, consequently increasing the cost of the turbine. So, it is desired that the problem be addressed without changing the design of the turbine.

Efforts towards obtaining a steady torque and increasing the power conversion by using a duct have been made separately. Ducts

* Corresponding author.
E-mail address: dhiman@iitm.ac.in (D. Chatterjee).

0960-1481/$ – see front matter © 2011 Elsevier Ltd. All rights reserved.
doi:10.1016/j.renene.2011.12.008

for flow augmentation have been developed by Ponta and Dutt [5]. Apart from the increase in captured power, use of an appropriate duct has many more advantages as explained in their paper. Setoguchi [6] has studied the effect of a brim type diffuser for hydrokinetic applications and proposed a design for two-way brim type diffuser for use in tidal streams, where the direction of the current changes with the tide.

Work concerning the duct/diffuser has been limited to seeing the highest flow speed that can be obtained in a duct for a given convergence ratio. A detailed study of the effects of a duct on a Darrieus turbine is lacking. The present study hopes to fill that space.

1.2. Scope

During the operation of Darrieus turbine, as a blade rotates around the axis, the torque produced by it varies. In fact, there may also be negative torque for a certain duration in the cycle. However, for the turbine to be useful, the torque averaged over the cycle has to be positive. Due to this variation in the blade torque with position, there is a variation—albeit reduced due to the summation of individual blade torques, in the turbine torque which is termed as torque ripple. The torque ripple can be reduced if a blade produces uniform torque over a longer duration of the cycle. There exist ducts that increase the power output by accelerating the stream. Our objective is to reduce the torque ripple while increasing the captured power. A duct has been designed to accomplish this. Subsequently, the effect of (*i*) the position of the turbine in the duct, (*ii*) the convergence angle of the duct and (*iii*) the external shape of the duct on the torque ripple and power conversion of the turbine is studied in an attempt to optimize the duct geometry.

2. Methodology

Experimental studies have clearly revealed that the flow through Darrieus turbine is extremely complex with simultaneous attached and separated flow regions as well as reattachment, dynamic stall and blade–vortex interaction. Hence appropriate choice of mathematical models for predicting the performance of Darrieus turbine is important and this is now taken up for discussion.

2.1. Choice of suitable mathematical approach

2.1.1. Momentum models

One category of modeling approach relies on the momentum principle. These momentum models [7] can be broadly classified into three and in the increasing order of complexity, these are — (*i*) single stream-tube model, (*ii*) multiple stream-tube model, and (*iii*) double multiple stream-tube model. These models have been proposed for studying wind turbines. Because of their geometry, the blades of a Darrieus turbine encounter the wake of the preceding blade. Of these models, (*i*) and (*ii*) do not consider the blade–blade interaction at all. In the double multiple stream-tube model, only the averaged effect of the upstream half of the cycle on the downstream half is considered. Darrieus wind turbines typically have very low solidity ($\approx$0.019–0.1 [8,9]). At such low solidities, the effect of the wake of one blade on the next is negligible. So, these models provide satisfactory results when applied to wind turbines.

2.1.2. Vortex models

Besides the momentum-based models described so far, vortex methods, employing free and bound vortices, are used to model the blade as well as the wake region of the turbine. Free vortex method requires the knowledge of aerodynamic coefficients obtained from static experiments. However, blades of Darrieus turbines undergo considerable changes in angle of attack under dynamic conditions. Additionally, there are problems of estimating circulation about a pitching aerofoil rotating in a circular path. So Ponta and Jacovkis [10] have combined free vortex method with finite element analysis of flow around the aerofoil. In their approach, thus, the free vortex model provides the boundary conditions for the finite element simulations.

Both the momentum-based stream-tube models and vortex methods are reasonably simple and less computationally expensive. However, these methods are not capable of accurately predicting physics beyond stall. Then two options exist — either to use semi-empirical models for post-stall phenomena which depends on experimental inputs or to carry out computational fluid dynamics simulations. The latter approach, though computationally more expensive, is a more reliable way of getting the flow physics without any need for free parameters. Such an approach has been adopted for Darrieus wind turbine in a recent paper by Amet et al. [11].

2.1.3. CFD model

Darrieus hydroturbines have higher solidities (0.15-0.4) as compared to wind turbines. The turbine used in this study, for example, has a solidity of 0.18. For such solidities, blade–blade interactions cannot be ignored and thus momentum-based models are not useful. For reasons stated above, vortex method is also not favoured. Hence, for Darrieus hydrokinetic turbine, it is felt, that complete computational fluid dynamics (CFD) simulation is needed.

In the present work, 3-D or shallow water modelling was not considered. The turbine is assumed to be located in an infinite expanse of water such that the effects of the changes in the surface level does not play any significant role. It may be added that the main focus in the present paper has been to identify the significant geometrical parameters of the duct and their influences on the performance of a turbine. Investigating 3-D effect is a part of future research.

2.2. Governing equations and numerical schemes

The basic equations that govern incompressible turbulent flow are the continuity and momentum equations given by:

$$\frac{\partial u_i}{\partial x_i} = 0 \tag{1}$$

$$\frac{\partial u_i}{\partial t} + u_j \frac{\partial u_i}{\partial x_j} = -\frac{1}{\rho}\frac{\partial p}{\partial x_i} + \nu \frac{\partial}{\partial x_j}\left(\frac{\partial u_i}{\partial x_j}\right) + \frac{\partial}{\partial x_j}\left(-\overline{u_i' u_j'}\right) + \chi \tag{2}$$

Eqn. (2) is known as the Reynolds-Averaged Navier–Stokes (RANS) momentum equation. $(-\overline{u_i' u_j'})$ is the Reynolds stress term that must be modelled using appropriate turbulence model in order to solve the "closure problem" [12]. It is known that k-ω model performs better than the k-ε model near the wall. However, there is one problem with k-ω model — its extreme sensitivity to the value of ω at irrotational boundaries of shear-flows. This led Menter [13] to formulate a hybrid model, which blends the advantages of k-ω model near the wall and k-ε model away from the wall. This model, termed as SST model, for Shear Stress Transport, performs satisfactorily in the decelerating boundary layer and is thus effective in predicting separation and hence was chosen as the suitable model. In the present work k-ω SST turbulence model is used. The transport equations for the k-ω SST model are given below [14]:

$$\frac{\partial(ku_i)}{\partial x_j} = \frac{\partial}{\partial x_j}\left(\frac{\Gamma_k}{\rho}\frac{\partial k}{\partial x_j}\right) + P + Y_k \tag{3}$$

$$\frac{\partial(\omega u_i)}{\partial x_j} = \frac{\partial}{\partial x_j}\left(\frac{\Gamma_\omega}{\rho}\frac{\partial \omega}{\partial x_j}\right) + G_\omega - Y_k + D_\omega \tag{4}$$

These equations were solved using commercial CFD solver, *Fluent*^{TM} which solves Navier–Stokes equations using finite volume technique. Details of the numerical models used and solver strategies adopted are given in Table 1.

2.3. Computational domain

Simulations were carried out for both ducted and unducted turbine geometries. Details of the turbine chosen for simulation are given in Table 2. This turbine was adopted from the experimental work by Kiho et al. [15]. Thus, this turbine geometry will serve dual purpose of bringing out the importance of proper duct design besides being used as a test case of validation. The two-dimensional computational domain for the unducted case, after determining the sensitivity of the domain size, extends 5D upstream and sideways and 10D downstream, where D refers to turbine rotor diameter.

Meshing of the computational domain is done using *Gambit*^{TM}. The mesh at the boundary layer region is refined enough so that the laminar sub-layer and the buffer layer are resolved and the wall function is not used. In order to achieve this meshing an orthogonal boundary layer mesh, with a first cell height that gives $y^+ < 5$, is used around the walls of the blade. Close up of the grid near the blade is shown in Fig. 1. This meshing approach together with the use of k-ω SST model ensures that near-wall features are well captured in the simulations. Rest of the domain is made up of unstructured quadrilateral and triangular elements. The transient sliding mesh technique [16–18] is used to simulate the rotating motion of the turbine rotor.

Boundary conditions applied to the model are as follows: a) velocity inlet at the upstream boundary, b) downstream boundary condition is pressure outlet, c) along the sides, stream-wise condition. The sub-domain containing the blades is set to rotate at different speeds and at each speed solution is continued until the initial transient behaviour vanishes and a periodic steady state is reached.

2.4. Determination of appropriate time-step and grid sizes

Before the actual simulations can be performed, it is necessary to determine the optimal grid size and time-step size that need to be used. Finer grids and smaller time steps might give a more accurate solution but, they increase the computational cost. So, the optimal values for these need to be found.

Grid sizing was determined from the consideration of spatial variations in the flow and from wall y^+ requirement of the turbulence model chosen. Thus, in sizing the grid, the y^+ requirement (<5) prescribed by the k-ω SST model was taken as the first constraint. Blade wall element size was chosen to give a reasonable cell aspect ratio (<10) for the first cell which will have the highest aspect ratio in a near-wall mesh. Boundary layer mesh was made around the blade. At increasing distances away from the walls, the element size increases smoothly. Finer grids were subsequently created by reducing the aspect ratio of first cell by reducing the element size of the blade walls.

For time step sensitivity study, a grid that is fine enough to capture flow physics was thus used. Time step size was then varied to determine an optimum time step size. Since in the present work, an implicit unsteady formulation is used. Hence there is no strict restriction (in the form of critical Courant number) on the time-step size due to the stability of the numerical scheme used.

The instantaneous torque of the unducted turbine at a tip-speed ratio (λ) of 2 was chosen as the case to determine the optimal time-step size. This particular tip-speed ratio was chosen because, as shown in Fig. 5 later, this value lies very close to the best efficiency point of the turbine. Simulations were performed for this tip-speed ratio with different time-step sizes and the resulting torque outputs were compared, as shown in Fig. 2.

It can be seen that after periodic convergence is reached there is no difference between the torques calculated by different time steps, except for small variation at the peaks. A non-dimensional time-step of 2.188×10^{-3} is sufficient to get an accurate solution and thus, further simulations were carried out with this.

Fig. 3 shows the variation of the torque with time for three progressively finer grids. It may be noted that this grid independence is shown for the ducted turbine as the ducted turbine poses greater challenge for meshing. It can be seen that there is virtually no difference in the solutions from grids 2 and 3 even though grid 3 is finer. Thus a mesh size equivalent to grid 2 is used for all simulations involving ducted geometry as it has been shown to be

Table 1
Numerical model and solver details.

Solution type	Sliding mesh
Transient	2nd order implicit
Turbulence	k-ω based SST
Pressure	2nd order
Momentum	2nd order
ω	2nd order
k	2nd order
P-V Coupling	Pressure based non-segregated

Table 2
Details of the turbine.

No. of blades	3
Blade Profile	NACA 63_3–018
Height	1.6 m
Rotor Diameter	1.6 m
Chord(Solidity)	0.3 m (0.179)

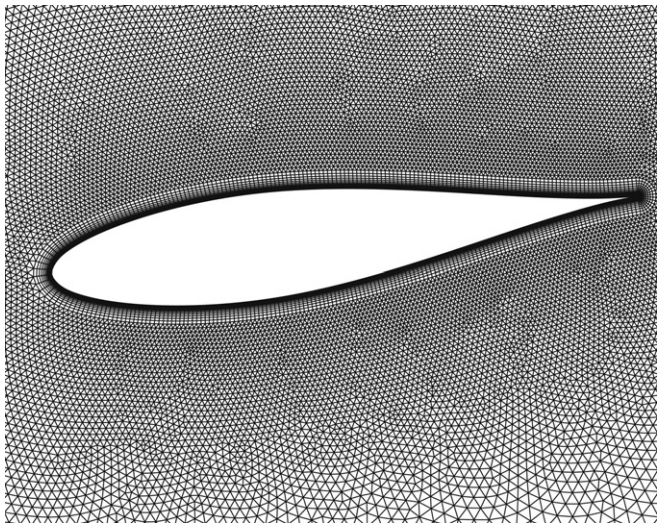

Fig. 1. Mesh around a turbine blade. Mesh near the wall is visible.

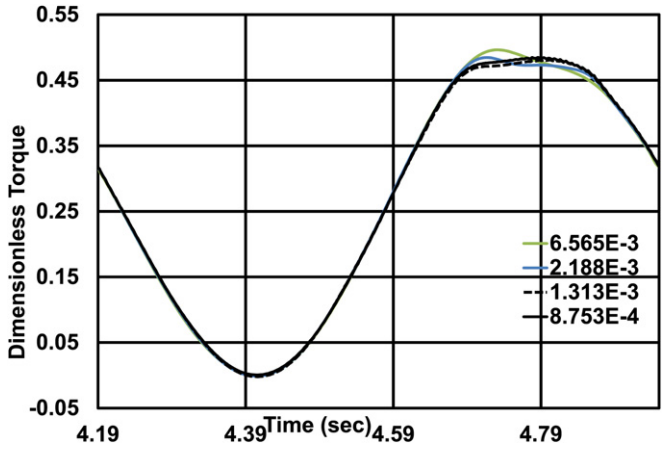

Fig. 2. Torque history for $\lambda = 2$ with various time step sizes, establishing time step size independence. Values in the legend are non-dimensional time-step size ($\Delta t/\tau$).

sufficient to get an accurate solution. For the unducted case, grid sensitivity analysis was done in a similar fashion and is not shown here for brevity.

2.5. Calculation of simulated variables

With the above mentioned parameters, numerical simulation was carried out. Post-processing of transient data reported in this paper needs some elaboration. At the very outset, it has to be ensured that the simulation is continued till the initial transience dies down and periodic steady state is reached. Fig. 4 shows the torque history for different turbine rotational speeds for a turbine without a duct. It can be seen that the torque has attained a periodic steady state in all the cases. It may be noted that as there are three blades in the turbine, repetition of the torque curve has three times the frequency of rotation of the turbine.

The instantaneous power generated by the turbine is equal to the product of the instantaneous torque (T) and the angular velocity (ω). This is not constant since the torque is not constant. Hence, in this paper two quantities are used to describe turbine performance with respect to torque variation. These are power coefficient (C_p) and torque ripple factor(TRF). Net power (P_T) averaged over a cycle

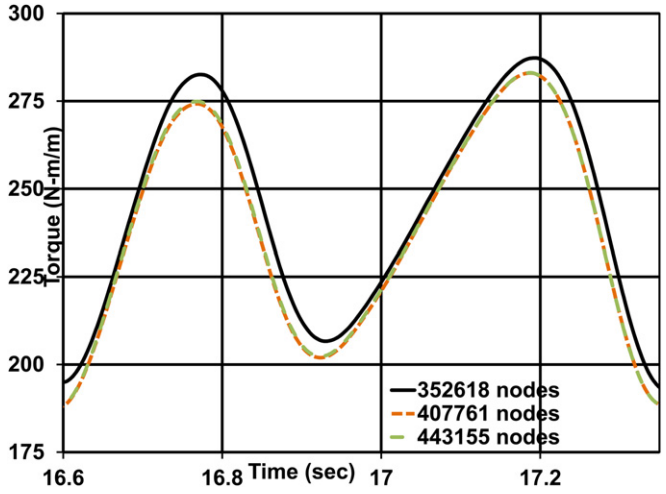

Fig. 3. Torque for three progressively finer grids, establishing grid independence.

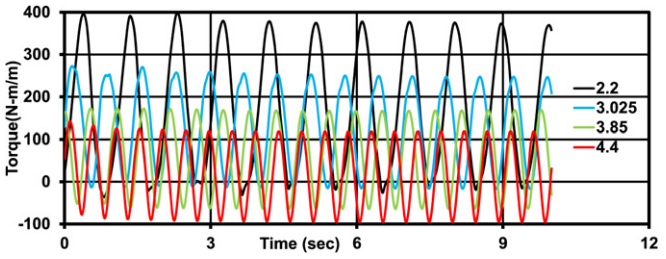

Fig. 4. Plot showing the torque per unit blade length versus time for different rotational speeds of the turbine.

is calculated as the product of average torque per cycle ($\overline{T}$) and rotational speed (ω).

$$\overline{T} = \frac{1}{\tau}\int_0^{\tau} T(t)\mathrm{d}t$$

$$P_T = \overline{T}\omega$$

Power coefficient is then defined as

$$C_p = \frac{P_T}{\frac{1}{2}\rho A V_\infty^3} \tag{5}$$

Here, A is the turbine frontal area equal to the product of the turbine diameter and height and V_∞ is the free stream velocity. This definition of C_p is used even for the the cases involving the use of a duct and needs some justification. It is clear that torque depends on fluid velocity and fluid velocity varies continuously inside the duct. It is also evident that the blades of Darrieus turbine, during one cycle, occupies a considerable length of the duct in front and behind the plane containing turbine axis. Thus power coefficient based on velocity at turbine centre is not a good descriptor. As power coefficient is a measure of conversion of kinetic energy, inlet area and free stream velocity combination is also not a good representative area and velocity scale. Since no other satisfactory definition exits, expression given in Eqn. (5), used extensively in unducted turbines, is employed here. In this sense, for the case of a ducted Darrieus turbine, Eqn. (5) is not a measure of performance but of the power produced.

Torque ripple factor is defined as ratio of the peak-to-peak amplitude of the instantaneous torque to the torque averaged

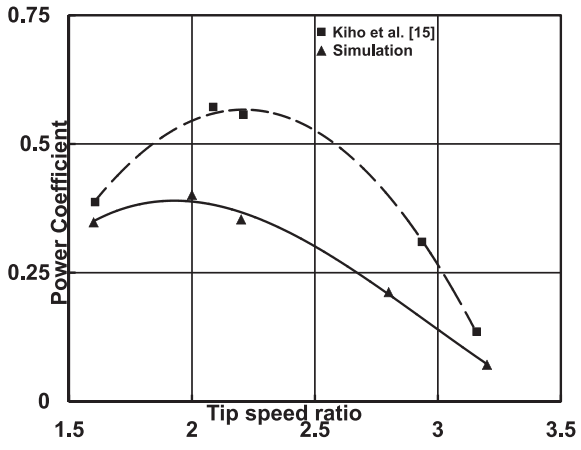

Fig. 5. Comparison of efficiency vs. tip-speed ratio obtained by Kiho et al. [15] and from the numerical model for validation of the model.

over one cycle, after periodic steady state is reached. This gives a dimensionless quantity representative of the variation in torque that can be compared across various turbines. When the torque produced is steady, the value of the ripple factor is 1. Torque ripple factor (TRF) is expressed as:

$$TRF = \frac{T_{pk-pk}}{\overline{T}} \tag{6}$$

where, T_{pk-pk} is the peak-to-peak amplitude of the instantaneous torque and $\overline{T}$ is torque averaged over one cycle.

2.6. Comparison of numerical prediction with experimental result

Before the predictions made by the CFD model can be considered, the numerical approach has to be validated by comparing it against experimental data. For this purpose, experimental observations of a straight-bladed Darrieus hydroturbine are required. Experimental observations of Darrieus hydroturbines along with the details of turbine geometry are scarce in literature. Only the observations made by [15] are available at this time. Hence, it is used to perform validation of the CFD model. They have measured the power output from an electrical generator driven by a three-bladed Darrieus turbine. By estimating the electrical and mechanical losses, the power at the turbine shaft was calculated, and from this the power coefficient (C_p) of the turbine was estimated and plotted against the tip-speed ratio. It is quite possible that the actual torque output may be somewhat different as errors may creep as the mechanical and electrical losses are not known explicitly and hence the trend, rather than exact values, can be compared. This is presented in Fig. 5. It is seen that there is a reasonable qualitative agreement with the experimental data of [15].

3. Design of duct

Ducts have been proposed, as mentioned in Section 1.1, to improve the performance of axial-flow turbines. However, not much effort is spent to analyse the role of duct geometry on the performance of Darrieus turbine.

In order to study the effect of duct on turbine performance, the turbine geometry is kept same as that mentioned in Table 2 earlier. Various ducts are designed keeping the dimension of the throat constant and varying the contraction ratio and convergence angle. Steady-state simulations without turbine geometry were carried out to determine the flow characteristics inside the duct. In contrast to the existing practice of placing the turbine at the throat of a duct, present approach examines the feasibility of placing the turbine not only at the throat region but also in the upstream (converging) portion. Because of this the flow is angled in towards the center and a higher angle of incidence of the flow, on the blade, is obtained. Fig. 6 shows a sketch of the duct along with the dimensions and also the relative position of the turbine in the duct for the first set of simulations with the duct. This particular duct is named as D01 in the present paper.

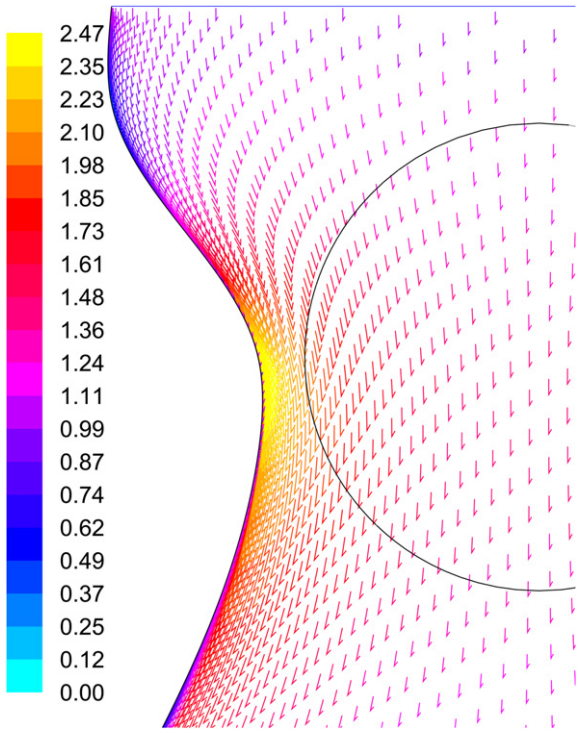

Fig. 7. Velocity vectors inside duct D01 without the turbine. The circle is the trajectory of the turbine blades.

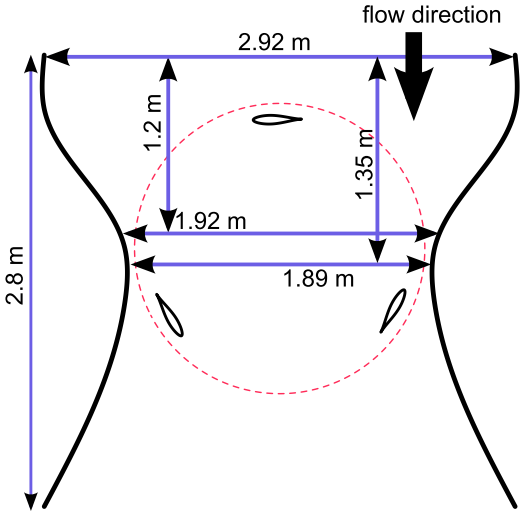

Fig. 6. Sketch of the duct (D01) and turbine along with the dimensions.

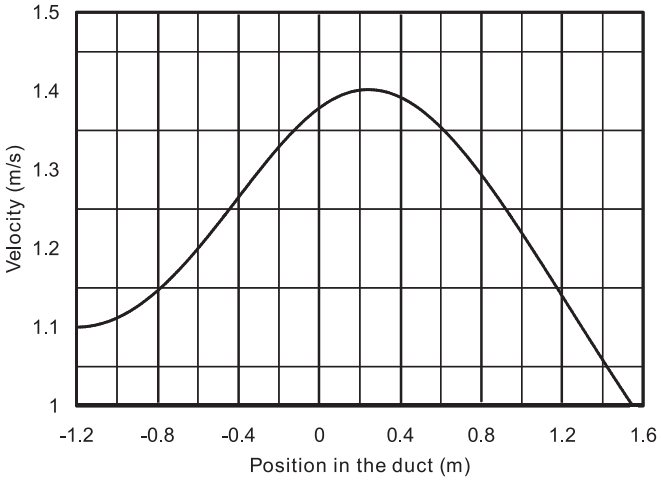

Fig. 8. Magnitude of velocity along the centerline of D01. Origin is chosen to coincide with the turbine centre and positive direction points to the downstream region of the turbine.

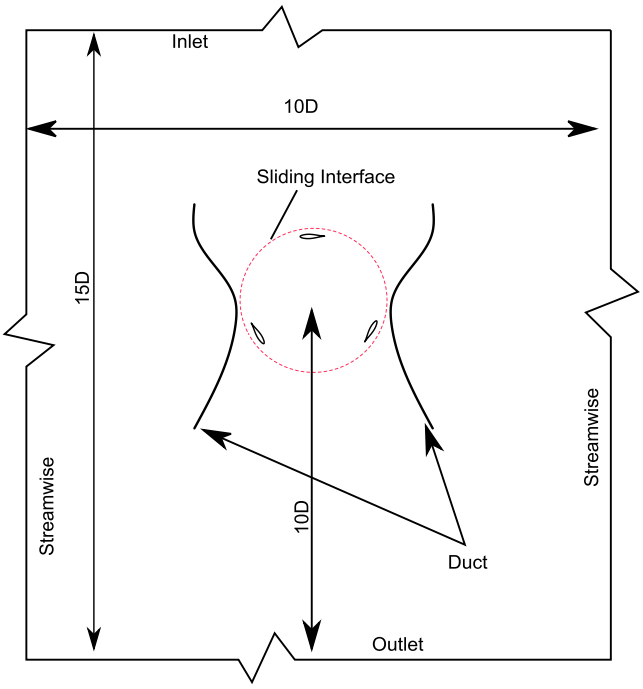

Fig. 9. Schematic of the computational domain in case of ducted turbine.

Fig. 7 shows the velocity vectors for the flow through duct D01 in the absence of the turbine. The change in direction as well as magnitude in the velocity field near the turbine trajectory can be seen clearly. The magnitude of velocity along the centerline of duct D01 in the absence of the turbine is shown in Fig. 8. The turbine is intended to be located such that its center coincides with the origin. From this it can be see that the location of the minimum area region (the throat) is downstream the point where the turbine is placed. This has a direct bearing on the ripple in the torque output as pointed out later.

4. Effect of duct

The domain of simulation along with all the boundary conditions is shown in Fig. 9. Simulations are performed for a range of speeds to capture the complete characteristics of the turbine.

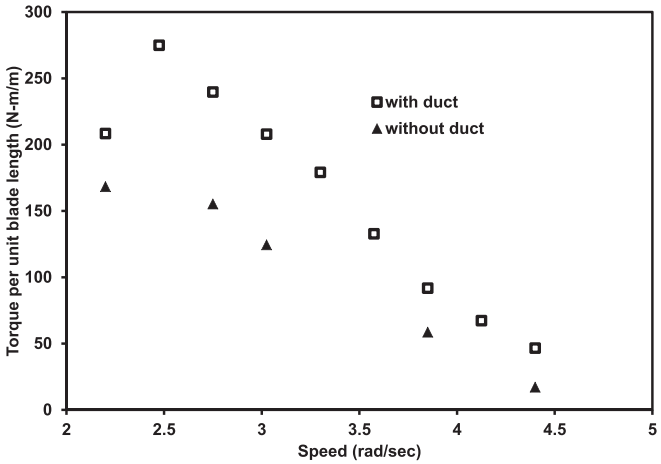

Fig. 10. Cycle-average torque vs rotational speed with and without duct for $V_\infty = 1.1$ m/s.

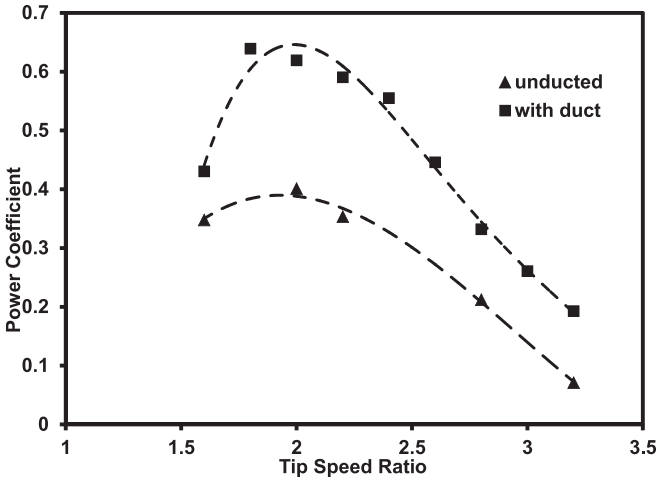

Fig. 11. The power coefficient of the turbine with and without the duct as a function of the tip-speed ratio for $V_\infty = 1.1$ m/s.

4.1. Torque and power characteristics

After the unsteady simulations have reached steady state, cycle-averaged torque output ($\overline{T}$) is determined. This is plotted against the rotational speed in Fig. 10. As expected, the power coefficient is higher with the duct (Fig. 11). The output is more in case of ducted turbine and hence a duct proves to be beneficial as far as C_p is concerned.

The torque output from a Darrieus turbine is not constant. Fig. 12 compares the instantaneous torque produced by the turbine with and without the duct for a duration of one cycle for $\lambda = 2$. It can be seen that there is a significant reduction of ripple in the torque output. Torque ripple factor (TRF) without the duct is 1.72, while with the duct TRF is only 0.41. That is, it is reduced by a factor of 4.15. Fig. 13

To get a better understanding of how the duct affects the torque ripple, the variation of torque in a single blade needs to be studied. Fig. 14 shows the variation in the torque of a single blade, with and without the duct. There are two main differences between the ducted and unducted case. First, in the upstream part of the cycle significant torque is produced over a longer duration and the peak is smaller in the ducted turbine in comparison with the unducted. Secondly and perhaps more significantly, there is a positive torque

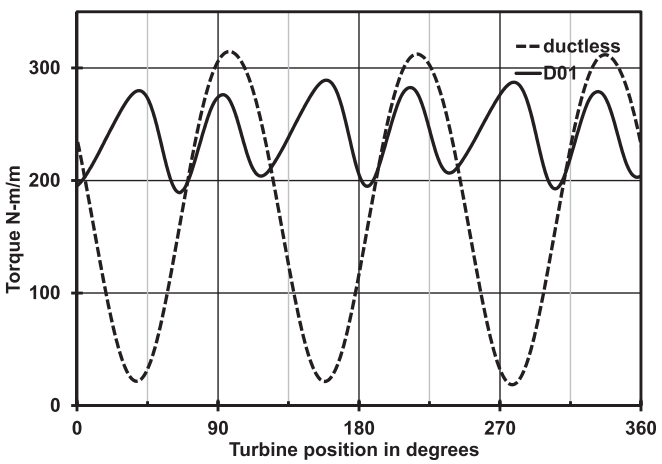

Fig. 12. Instantaneous torque vs. turbine position with and without duct for $\lambda = 2$ and $V_\infty = 1.1$ m/s.

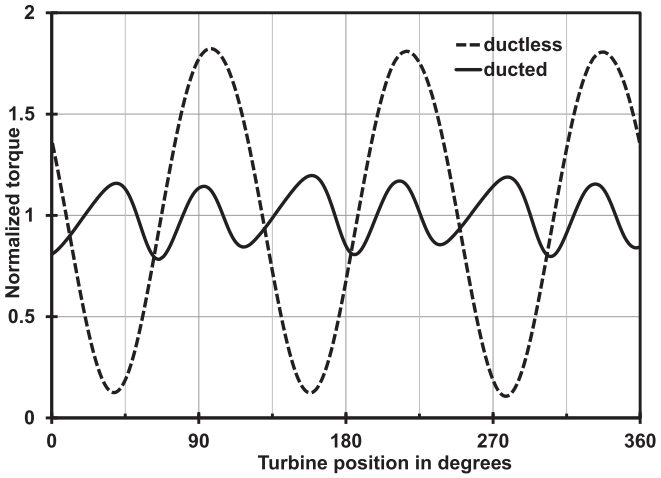

Fig. 13. Normalized torque vs. turbine position with and without duct for $\lambda = 2$ and $V_\infty = 1.1$ m/s.

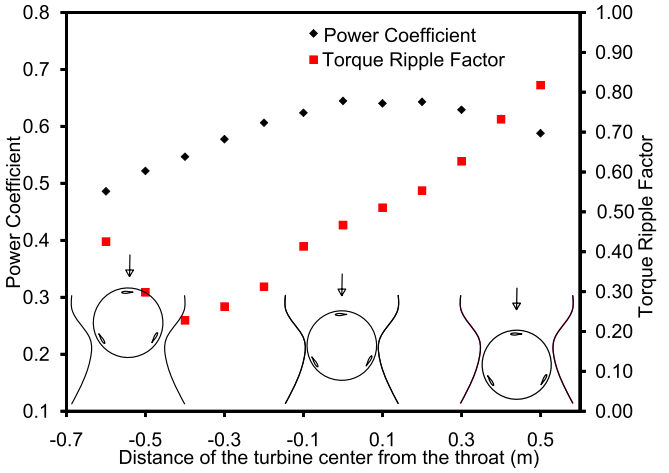

Fig. 15. Variation of power coefficient and ripple factor with the position of the turbine in the duct.

in the downstream part of the cycle as well for the ducted turbine whereas the unducted turbine shows negative (retarding) torque.

Within the cycle, the torque produced by a blade depends on the relative velocity and the angle of attack of the blade. The turbine is placed in the duct such that the upstream half of the Darrieus turbine is in a region where the flow is converging. The magnitude of the stream velocity increases until the throat is reached. Because of this velocity gradient and converging flow, torque is produced earlier and for a longer duration of the cycle. Also, the duct is located upstream of the throat, so the velocity tends to increase even in the rear half of the turbine. This is expected to compensate the effect of the wake induced velocity downstream of the preceding blade. This leads to a greater positive torque for $180° < \theta < 360°$ (Fig. 14). Due to a combination of these two changes, the torque ripple is reduced.

4.2. Effect of turbine location and duct geometry

It may be noted here that the reduction of torque ripple by a factor of 4.15 and improvement of power coefficient by a factor of 1.5 was obtained for a given turbine location. These quantities may be improved further by properly choosing turbine location inside the duct and the duct geometry. This is now taken up for discussion.

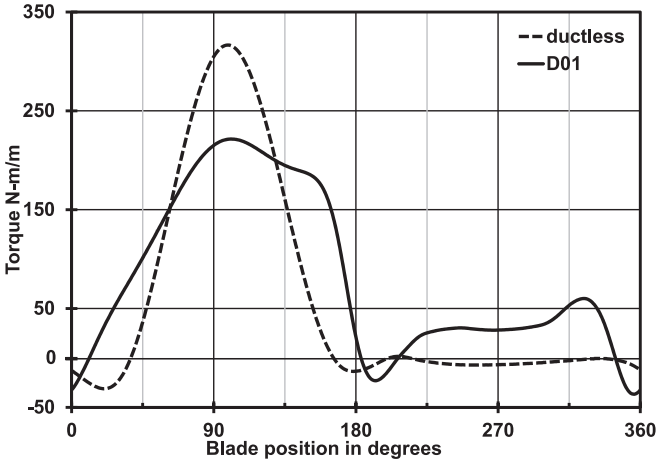

Fig. 14. Blade torque vs. blade position with and without duct for $V_\infty = 1.1$ m/s.

4.2.1. Position of the turbine in the duct

The effect of changing the position of the turbine in the duct is studied by performing simulations with the turbine at various locations in the duct, for a tip-speed ratio of 2. Power coefficient and torque ripple are calculated in each case and plotted (Fig. 15). It can be seen that the power coefficient is maximum when the turbine center is 0.1 *m* from the duct inlet, which coincides with the throat of the duct. And, the torque ripple factor is least when this distance is 0.9 *m*, that is, the turbine center is 0.4 *m* upstream the throat.

Thus the ideal location for the turbine is going to be between 0.9 and 1.3 *m* from the duct inlet. Looking only at the power coefficient it is best to place the turbine such that the turbine center is 1.3 *m* from the duct inlet, that is, at the throat. Though, torque ripple should also be low at the chosen position. This needs an optimization of the geometry which was not attempted in this work. By moving the position of the duct, as far as the turbine is concerned, there are two factors that are changing. They are (*i*) the absolute velocity of the stream and (*ii*) the angle of incidence on the blades. The stream velocity in the duct is going to be highest at the narrowest portion of the duct as a result of the continuity equation. And so it is expected that when the turbine is placed in this position the power conversion by the turbine will be maximum because the

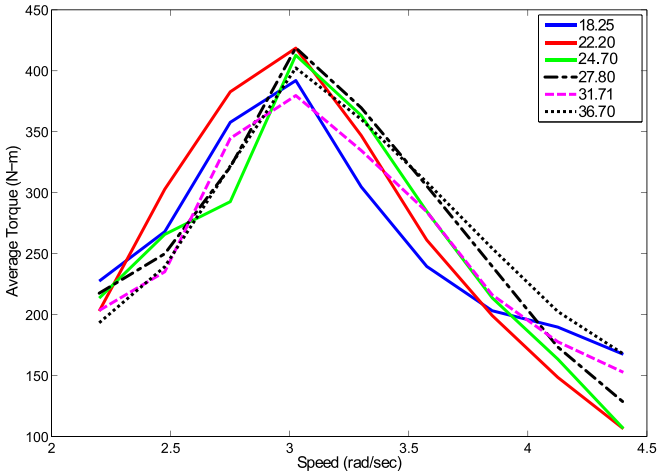

Fig. 16. Torque vs. Speed for ducts with different convergence angles. Values in legend are half-angles.

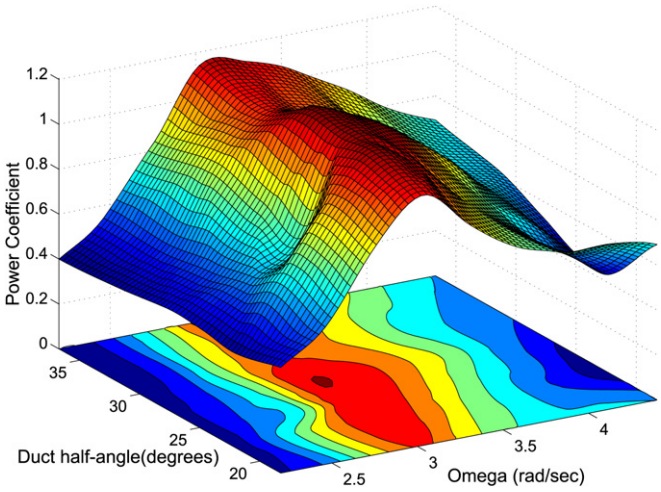

Fig. 17. Variation of the power coefficient with duct half-angle and speed.

power converted varies as a cube of the stream speed. By looking at Fig. 15 it can be verified that this is indeed the case — the power coefficient is the maximum when the turbine center is at the narrowest section of the duct. Influence of angle of incidence is studied by suitably varying the convergence angle of the duct.

4.2.2. Convergence angle of the duct

In continuation of the investigation of the effect of duct parameters, the effect of the convergence angle of the duct is studied next. Six ducts with the same inlet width of 4.32 m but with convergence angles ranging from 18° to 36° are modelled and simulations are performed to obtain the power and torque characteristics. The length of the upstream portion is changed to change the convergence angle of the duct. The other option of changing the duct angle is to keep the length of the duct constant but change the inlet width, so that the angle changes. This directly affects the speed of the flow near the turbine. The only side effect of the procedure used here is that there is going to be a small change in the friction loss in the upstream part for each case since the length of the upstream part is changing while the downstream portion is not changed.

Fig. 16 shows the torque characteristics of the turbine for various duct convergence angles. It can be seen that in all the cases, the

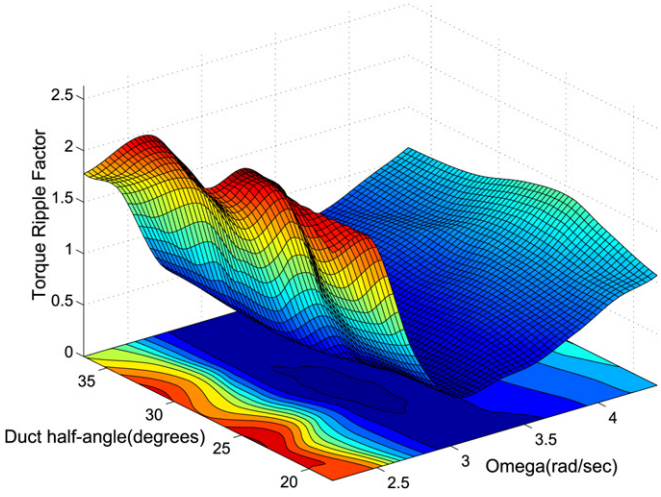

Fig. 18. Variation of the torque ripple factor with speed and convergence angle.

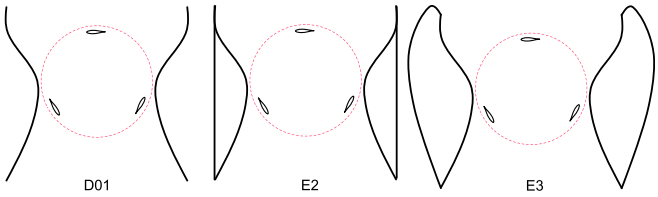

Fig. 19. The different external shapes for which the simulations were performed.

peak torque occurs at the same speed. This is understandable since the duct contraction ratio is kept constant so that the the same velocity through the turbine is obtained for each angle. The power coefficient and torque ripple factor are shown in Figs. 17 and 18 respectively after surface fitting using cubic interpolation. From Fig. 17 it can be seen that there is a maximum for the power coefficient at duct half-angle of 27° and $\omega \approx 3$ *rad/s*. Secondly, it is observed that the speed at which the peak power conversion is observed does not change with the duct half-angle. As far as the torque ripple is concerned, there is a minimum at approximately the same coordinates where power coefficient was highest. The gradient here is very gentle and the minimum is not visible in the plot. Extending the range of the duct half-angle on both sides will show it clearly. Looking at Figs. 17 and 18 it is observed that the speed of about 3 *rad/s* for peak power coefficient and lowest torque ripple is the same. Hence, it can be said that the turbine should operate at this speed.

4.2.3. External shape of the duct

In order to see the effect of the external shape of the duct on the turbine output, simulations are carried out with ducts that have the same internal shape but three different external shapes, shown in Fig. 19. The shape of the duct used earlier in Section 4.1 is used here for the internal shape. Since the duct simulated earlier already has a concave shape, the results obtained then are taken as representative of a duct with a concave exterior.

Figs. 20 and 21 show the power coefficient and ripple factor respectively for these three ducts. It is observed that the external shape has less effect on the torque ripple, with E3 showing slightly higher TRF in comparison to other ducts. Power coefficient on the other hand, is highest for the duct which has a straight line as outer

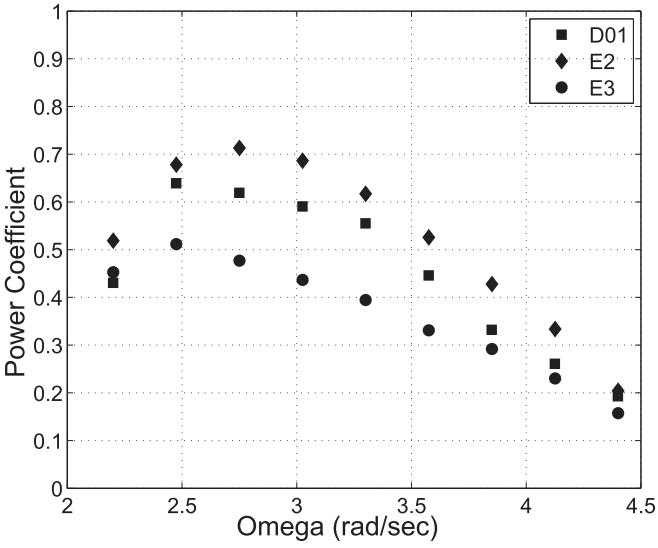

Fig. 20. Power coefficient vs. Speed for duct with different external shape.

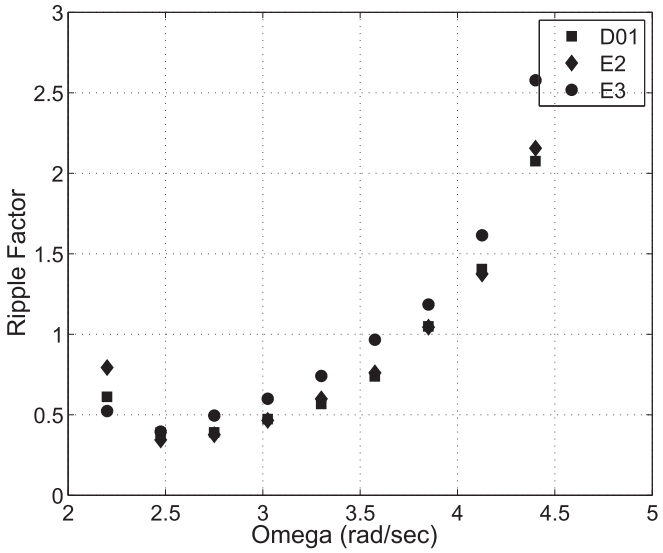

Fig. 21. Comparison of torque ripple factor for three ducts, at various speeds.

shape and lowest for a duct with convex outer shape. The duct with a convex outer shape has the lowest power coefficient. The reason for this is the difference in the separated zones attached to the ducts' exterior. The duct with the straight external shape (E2) has the lowest back-pressure of the three, so the flow-rate through it is highest and consequently the power produced is more. This is in agreement with the experimental observations by [6], that show that highest flow velocity in the duct is obtained for the duct with a straight outer shape.

5. Conclusions

A duct for Darrieus turbine has been designed and its effect on the output of the turbine has been simulated. The results reveal that it is possible to improve the performance of Darrieus turbine on multiple fronts using an appropriately designed duct. An attempt was made at optimizing the shape of the duct by studying the effect of the position of the turbine, the convergence angle of the duct and the external shape of the duct on the output of the Darrieus turbine. It was observed that these parameters have an optimum value. The main conclusions from this study are listed below:-

- Effect of Duct: At $\lambda = 2$, by using a duct, the torque ripple is reduced by a factor of 4.15 and the power conversion factor is increased to 0.63 from 0.40.
- Turbine position in the duct: Lowest torque ripple is 0.27 when the turbine center is 0.4 m upstream of the throat. C_p is maximum, $= 0.644$ when the turbine is at the throat.
- Duct convergence angle: Maximum power coefficient and lowest torque ripple are obtained at the same value of duct half angle, equal to 27° The dependence of the power coefficient and torque ripple on duct convergence angle is weak.
- External shape: The duct with straight external shape is observed to have best performance with a peak power coefficient of 0.72, while the convex external shape has a peak of only 0.51.

5.1. Scope for future work

Present paper has brought out the importance of duct design on the performance of Darrieus water turbine. Further work needs to be carried out to determine:-

- The effect of turbine-duct clearance, blade pitch, and length of the duct throat.
- The effect of the duct on the starting characteristics of Darrieus turbine.
- Designing a bi-directional duct that incorporates the advantages of the duct presented here.
- Effect of free surface on the performance of the Darrieus hydroturbine for shallow water applications

Acknowledgements

The authors would like to thank High Performance Computing Environment (HPCE), Computer Centre, Indian Institute of Technology Madras for providing the computational resources required to perform the simulations in this paper. The authors also thank the reviewers whose comments have helped in improving the quality of the paper.

References

[1] Khan MJ, Bhuyan G, Iqbal MT, Quaicoe JE. Hydrokinetic energy conversion systems and assessment of horizontal and vertical axis turbines for river and tidal applications: a technology status review. Applied Energy 2009;86:1823–35.
[2] Gorlov A. The helical turbine: a new idea for low-head hydro. Hydro Review 1995;14(5):44–50.
[3] Gorban AN, Gorlov AM, Silantyev VM. Limits of the turbine efficiency for free fluid flow. Journal of Energy Resources Technology 2001;123:311–7.
[4] Bernad S, Georgescu A, Georgescu SC, Susan-Resiga R, Anton I. Flow investigations in Achard turbine. Proceedings of the Romanian Academy 2008;9(2).000–000.
[5] Ponta F, Dutt GS. An improved vertical-axis water-current turbine incorporating a channelling device. Renewable Energy 2000;20:223–41.
[6] Setoguchi T. Development of two-way diffuser for fluid energy conversion system. Renewable Energy 2004;29(10):1757–71.
[7] Islam M, Ting DS, Fartaj A. Aerodynamic models for Darrieus-type straight-bladed vertical axis wind turbines. Renewable and Sustainable Energy Reviews 2008;12:1087–109.
[8] Consul CA, Willden RHJ, Ferrer E, Mcculloch MD. Influence of solidity on the performance of a cross-flow turbine. In: Proceedings of the 8th European Wave and tidal energy Conference, Uppsala, Sweden; 2009.
[9] Dominy R, Lunt P, Bickerdyke A, Dominy J. Self-starting capability of a Darrieus turbine. Power and Energy 2007;221:111–20.
[10] Ponta FL, Jacovkis PM. A vortex model for Darrieus turbine using finite element techniques. Renewable Energy 2001;24:1–18.
[11] Amet E, Maître Thierry Pellone C, Achard JL. 2D numerical simulations of blade-vortex interaction in a Darrieus turbine. Journal of Fluids Engineering 2009;131(11):1111031–11110315.
[12] Wilcox D. Turbulence modeling for CFD. CA: DCW Industries Inc; 1993.
[13] Menter F. Two-Equation Eddy-Viscosity turbulence models for engineering applications. AIAA Journal 1994;32(8):1598–605.
[14] Prem Kumar T, Chatterjee D. Numerical study of turbulent flow over an S-shaped hydrofoil. Proceedings of the Institution of Mechanical Engineers, Journal of Mechanical Engineering Science, Part C 2008;222:1717–34.
[15] Kiho S, Suzuki K, Shiono M. The power generation from Tidal currents by Darrieus turbine. In: World Renewable energy Conference; 1996. p. 1242–5.
[16] Shekhar SM, Jayanti S. CFD study of power and Mixing time for Paddle Mixing in Unbaffled Vessels. Chemical Engineering Research and Design 2002;80(5):482–98.
[17] Aubin J, Fletcher D, Xuereb C. Modeling turbulent flow in stirred tanks with CFD: the influence of the modeling approach, turbulence model and numerical scheme. Experimental Thermal and Fluid Science 2004;28(5):431–45.
[18] Fluent 6.3 User's Guide. Fluent Inc; 2006.